13

Formation of thin-film resist materials based on organotin oxoclusters promising for electron-beam and extreme ultraviolet nanolithography

© M.Yu. Zakharina,[1] K.V. Arsenyeva,[1] M.A. Baten'kin,[1] A.N. Konev,[1] R.S. Kovylin,[1] A.A. Lokteva,[1] A.E. Pestov,[2] A.N. Nechai,[2] A.Ya. Lopatin,[2] A.A. Perekalov,[2] S.A. Chesnokov,[1] A.V. Piskunov,[1] I.L. Fedushkin[1]

[1]G.A. Razuvaev Institute of Organometallic Chemistry of Russian Academy of Science (IOMC RAS), 603950 Nizhny Novgorod, Russia
[2]Institute for Physics of Microstructures of the Russian Academy of Sciences, branch of Federal State Budgetary Scientific Institution „Federal Research Center Institute of Applied Physics of the Russian Academy of Sciences" 603087 Afonino, Kstovsky District, Nizhny Novgorod Region, Russia
e-mail: m.zakharina@mail.ru, sch@iomc.ras.ru

Received April 25, 2025
Revised October 14, 2025
Accepted October 15, 2025

Conditions for the formation of 10−60 nm thick films on the surface of a single-crystal silicon substrate from organic solutions of alkyl and non-alkyl tin oxoclusters TOC-21 and TinS have been developed. The surface roughness of TOC-21 films is less than 1 nm. Exposure of the films to an electron beam or radiation with a wavelength of 13.5 nm enabled the formation of microstructures of a tin-containing substance on the substrate surface. The results can be used to develop tin-containing resists for electron-beam and extreme ultraviolet (EUV) nanolithography.

Keywords: oxo cluster, negative photoresist, thin films, electron beam- nanolithography, EUV- nanolithography.

DOI: 10.61011/TP.2026.02.62892.85-25

Introduction

Production of integrated circuits with topological features smaller than 10−20 nm with high charge density and low roughness of line edges has required a transition of lithographic processes from deep ultraviolet (193 nm or 248 nm) to electron-beam lithography and extreme ultraviolet lithography (EBL and EUVL) [1,2]. In this context, studies of the EBL and EUVL processes themselves, and creation of resists satisfying the requirements of these processes has become important [3].

One of well known electron-beam resists suitable for achieving a resolution lower than 10 nm by the EBL method is currently the XR1541 negative resist. The resist is hydrogen silsesquioxane (HSQ), a polymer silicon-inorganic compound. According to the datasheet, the required resist exposure dose is 400−700 μC/cm^2 (200 eV−100 keV) depending on the film thickness (30−180 nm), thin-film resolution is 6−10 nm [4]. Employment of the XR1541 resist in EBL techniques is discussed in many papers by both foreign and Russian authors [5–9]. Studies focus on increasing the sensitivity, resolution, contrast ratio and reducing the line edge roughness, critical size of exposed structures, and proximity effect. Authors of [10] report that resist sensitivity depends on film thickness: the thinner the film the greater the required exposure dose; thus, when a resist layer thickness is 55 nm, the sensitivity is 311 μC/cm^2, and the lowest sensitivity, 887 μC/cm^2, was recorded for a 5 nm layer. It is shown in [11] that a decrease in the development temperature can significantly reduce the line edge roughness, and non-monotonic dependence of resist contrast on development temperature was also identified. The effect of developer and temperature at various development stages on the contrast, sensitivity and etching resistance are also discussed in [12–14]. High selectivity of HSQ in plasma-chemical and reactive ion etching conditions, and HSQ suitability for creating nanoelectronic device prototypes with sizes up to 10 nm were demonstrated [15,16]. The resist was also successfully tested on EUV lithography machines. Resist sensitivity with a thickness of 70 nm is estimated as 11.5 mJ/cm^2 with a contrast ratio of 1.64 [17].

Oxo-cluster compounds containing metals with high atomic radiation absorption cross-section for a wavelength in the neighborhood of 13.5 nm (Sb(V), Cr(III), Fe(III), Co(III) and In(III)) are considered as promising materials for producing negative resists capable of satisfying the requirements of both electron-beam and EUV lithography [3,18]. Tin-containing metal complexes containing Sn–C-alkyl bonds are being studied most extensively [19–21]. Non-alkyl tin derivatives are most preferable because alkyl derivatives are highly toxic and have an extremely negative influence on human health and environment. Clusters, where alkyl groups are replaced with easily dissociating inorganic ligands (for example, halide ions), are the most safe. The literature describes synthetic approaches to non-alkyl tin-oxo clusters using low-toxic inorganic precursors [22]. Efforts are focused on developing techniques for synthesizing metalorganic compounds and nanoclusters on the

basis thereof, and on evaluating metalorganic compounds as resists for EBL and EUV nanolithography [19,23–26]. Cation tin-oxo clusters with various anions were used as a basis for producing negative resist films 40 nm in thickness, whose sensitivity in EUV experiments is $34-50\,\mathrm{mJ/cm^2}$. To obtain topological features in the form of lines with a half-step of 50 nm depending on the patterning conditions, a radiation dose from 34 to $131\,\mathrm{mJ/cm^2}$ is required [27]. Sensitivity of tin-containing resists with the same thickness studied in [19] is within $180-690\,\mathrm{mJ/cm^2}$ and is defined both by the origin of anion and by the origin of substituent bound to a tin atom. Efficiency of patterning via non-alkyl tin-oxo clusters by the EBL technique was estimated in [28]. Reactivity of tin-oxo cluster is exhibited at a dose equal to $100\,\mu\mathrm{C/cm^2}$. Sharp lines 50 nm in thickness were obtained at a dose equal to $1000\,\mu\mathrm{C/cm^2}$. In addition, the study shows the influence of structural properties of a cluster (origin of ligand and number of tin atoms in the compound) on resist resolution and sensitivity.

Analysis of the literature data concerning the synthesis of metalorganic compounds and nanoclusters, and evaluation of metalorganic compounds as resists suitable for EBL and EUVL nanolithography were accomplished only by foreign authors. At the same time, one of the priority tasks in Russia is to create domestic microchips, for which not only domestic EBL and EUVL machines shall be created, but also domestic resits fully satisfying the requirements of these machines shall be developed. Therefore such studies are especially important.

This work is the first stage of study of alkyl and non-alkyl tin-containing clusters as feedstock for producing resists, i.e. determining conditions for formation of thin films on the basis of tin-containing clusters on single crystal silicon wafers and testing the obtained films for electron-beam and EUV radiation sensitivity ($\lambda = 13.55\,\mathrm{nm}$). The obtained data can be used as a basis for further work on synthesis and investigating new types of organotin-oxo clusters designed for EBL and EUVL applications.

1. Experimental

Oxo clusters

$$Sn_{14}(\mu_3\text{–}O)_{12}(\mu_2\text{–}O)_4(\mu_2\text{–}OH)_4(PZ)_8(HPZ)_4Cl_{12}\ \text{(TOC-21)}$$

and

$$[(C_4H_9Sn)_{12}O_{14}(OH)_6]^{2+}[PTSA^-]_2\ \text{(TinS)}$$

were produced using techniques described earlier in [22,29].

Films were deposited on the substrate from TOC-21 and TinS oxo cluster solutions by spin-coating during 30 s. 1A2KDB-10 single crystal silicon wafers with the (111) orientation were used as substrates. AFM method was used to determine wafer surface roughness before film deposition. Wafer surface roughness was $Ra \approx 0.2\,\mathrm{nm}$.

Oxo cluster solutions were prepared in ethyl lactate („Aldrich") and 2-butanone („Reachim"). Oxo cluster concentration was varied within $5-13\,\mathrm{g/l}$. TOC-21 solution in ethyl lactate was additionally ultrasonicated (20 kHz) during 20 min. Insoluble residue was filtered via a $0.2\,\mu\mathrm{m}$ PTFE filter. TinS solution in 2-butanone was boiled at 90 °C until complete dissolution of the oxo cluster. To obtain films with the desired thickness, spin coater speed („Spincoat G3-8") was varied from 300 to 3000 rpm.

To remove residual solvent, films formed on the wafer were dried during 3 min, 70 °C. Film thickness was measured by the ellipsometry method (META-900 ellipsometer).

Analysis of surface microrelief and surface roughness (R_q) on a $2 \times 2\,\mu\mathrm{m}$ film fragment was performed using the Solver-P47 atomic force microscope (Russia).

After exposure, films were developed by rinsing in a 3/2 isopropanol/water mixture during 30 s and then dried at 50 °C during 2.5 min. Pre-/post-exposure and pre-/popst-development SEM images of wafer sample surfaces with films were made on the Regulus SU8100 (Hitachi, Japan) scanning electron microscope equipped with the XFlash® 6 | 60 (Bruker, Germany) energy-dispersive microanalysis (EDS) system. Samples were studied without conducting coating. Analysis of the obtained relief was performed at an accelerating voltage of 1 kV to avoid charge accumulation on the sample.

Surface modification of wafers with films of various origin irradiated by extreme ultraviolet were examined using the SuperView W1 (China) optical white light microinterferometer. Since the oxo cluster film is transparent to visible wavelength range, profiles of the developed surfaces were examined using the interference techniques after deposition of a tungsten coating (30 nm) on samples by the magnetron sputtering technique. Thickness of the deposited coating was estimated using a „witness standard" (a 0.5 mm standard silicon wafer was placed during sputtering in the immediate vicinity to the sample). Coating thickness on the witness standard was measured by the small-angle X-ray diffraction method on the PANalytical XPert PRO (Netherlands) diffractometer. The coating is opaque to visible light and simultaneously doesn't damage the sample surface relief.

Electron-beam exposure of wafers with films was performed using the Regulus SU8100 (Hitachi, Japan) scanning electron microscope. The following operating settings were used for the microscope: accelerating voltage - 30 kV, 250x and 2500x magnification, flange focal length - 8 mm, emission current - $10\,\mu\mathrm{A}$, electromagnetic lens mode - High (Condencer 1), scanning mode - slow 5.

Extreme UV exposure at 13.55 nm of wafer samples with films was performed on a laser-plasma source bench. The experimental bench setup is shown in Figure 1.

Radiation of Nd:YAG laser *1* with a wavelength of 1064 nm, pulse duration of 9 ns, pulse energy of 0.8 J, pulse repetition rate of $5-10\,\mathrm{Hz}$ was focused using a short-focus lens on a gas jet coming from pulse nozzle *2*; laser pulse repetition rate was synchronized with the nozzle valve opening frequency. Pulse nozzle was used to facilitate

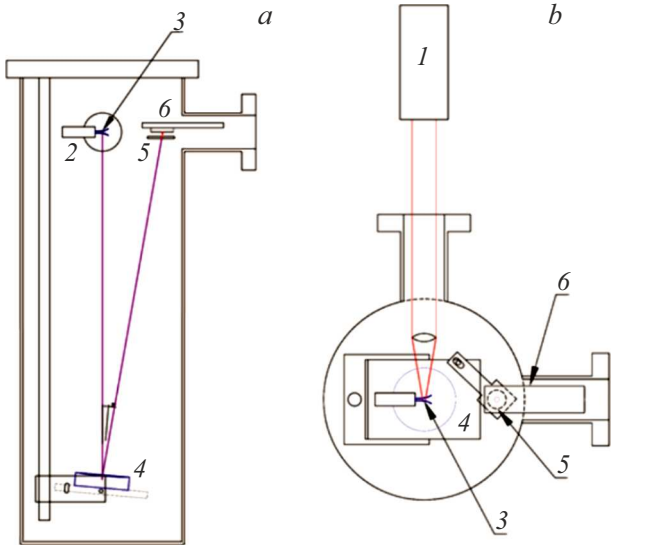

Figure 1. EUV irradiation experiment setup ($\lambda = 13.55$ nm): *a* — side view; *b* — plan view. *1* — Nd:YAG laser, *2* — pulsed gas nozzle, *3* — laser spark, *4* — multilayer EUV mirror, *5* — EUV filter, *6* — sample mounted on a linear translation stage.

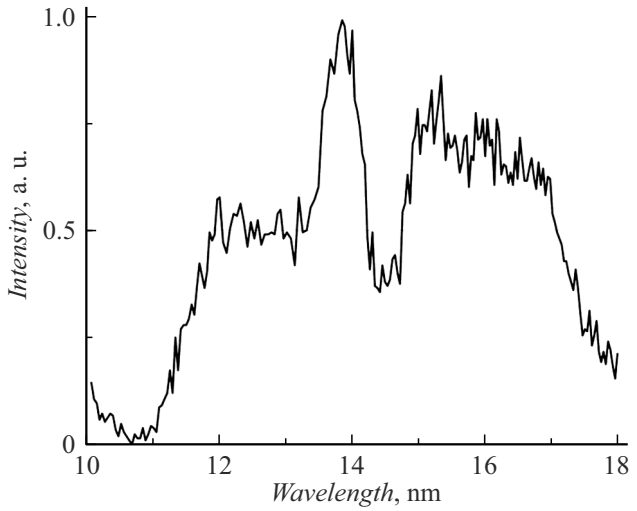

Figure 2. Gas-target laser-plasma source radiation spectrum (Ar).

gas evacuation from the vacuum volume. Laser radiation interaction with gas atoms induces multiple ionization followed by recombination radiation of multicharged ions from laser spark *3*. Working gas, Ar, (gas inlet pressure at the nozzle was 10 atm) and ArVIII radiation were used to produce 13.55 nm radiation. Ar gas target radiation spectrum excited by Nd:YAG laser radiation is shown in Figure 2.

Gas target radiates at 4π sr and, as can be seen, there is a quite broad spectrum. To collect a significant portion of emitted power and isolate a desired wavelength (13.55 nm), spherical multilayer (Mo/Si) collecting monochromator mirror *4* was mounted at 5° to the incident radiation axis. Transmission band of the mirror in absolute values of reflection coefficient is shown in Figure 3. Mirror diameter was 50 mm, distance to the source was 320 mm, thus, a solid angle cut by the collector was $\Omega = 0.02$ sr.

Radiation collected by the monochromator mirror and transmitted through thin-film absorption filter *5* was focused on wafer with the test film *6* mounted on the linear translation stage. Thin-film absorption Be filter passes operating wavelength radiation and cuts off background visible and ultraviolet radiation contained in the laser spark radiation spectrum. Filter transmission spectrum is shown in Figure 4.

Several points with different absorbed doses can be formed on the resit wafer during one evacuation of the vacuum system by moving the sample using the linear

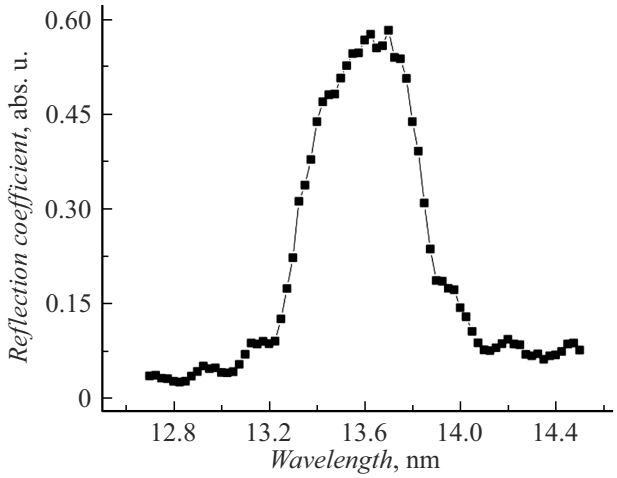

Figure 3. Spectral dependence of reflection coefficient of the multilayer monochromator mirror. Multilayer Mo/Si structure with the period $d = 6.9$ nm and number of periods $N = 50$.

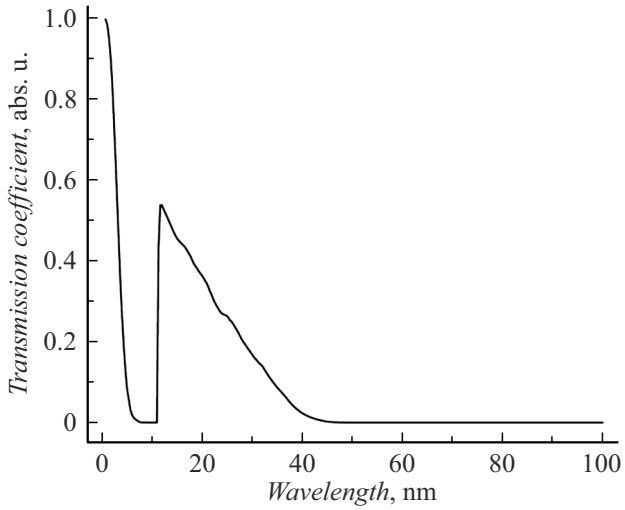

Figure 4. Spectral dependence of the transmission coefficient of the thin-film absorption filter — 500 nm Be film, calculation [30].

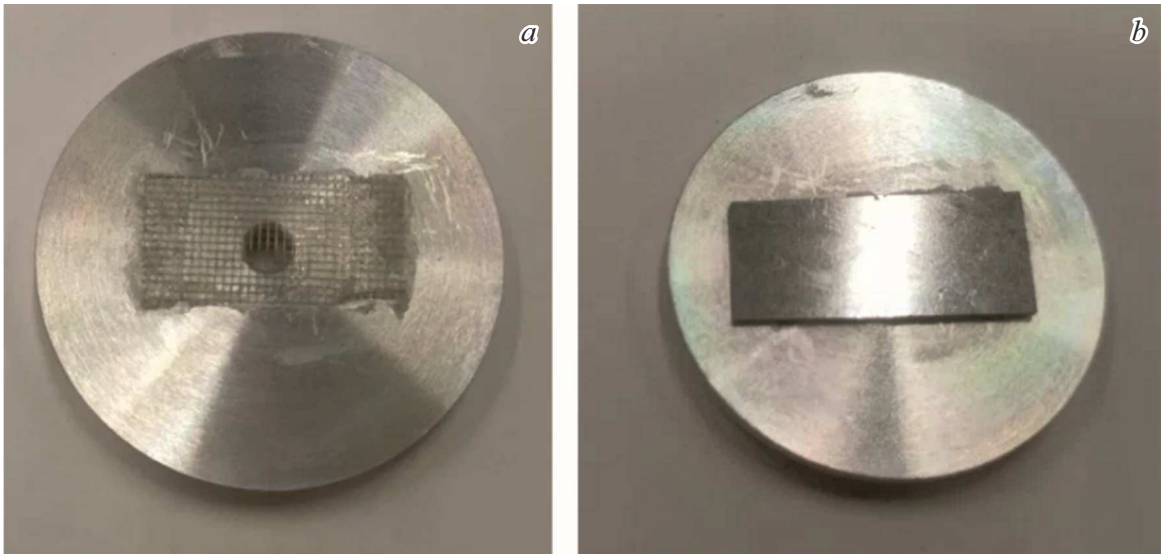

Figure 5. Sample holder photograph: *a* — with attached masking mesh; *b* — with attached sample.

translation stage. The number of points is defined by the ratio of EUV radiation spot on the sample and sample size.

Focusing spot size in this bench configuration determined in [31] was approximately equal to 0.5×1.0 mm.

To estimate the EUV radiation dose in the spot, the FDUK-100UV EUV radiation detector (spectral sensitivity of which was measured at PTB Metrology Institute (Berlin, Germany) [32]) with additional double-filter unit was placed in the monochromator focusing region to suppress spurious exposure by radiation reflected from the chamber walls and falling into the detector aperture, signal captured by the detector was recorded and radiation power was estimated by the signal value.

Detector was operated in current mode, and a signal at the detector downstream of the monochromator mirror optimized to $\lambda = 13.55$ nm was $I_{det} = 5.5 \cdot 10^{-5}$ A.

Taking into account the parameters of the X-ray optical scheme, including the spectral sensitivity of the detector and the transmission coefficient of the filter, the radiation power can be estimated using equation $P_{det} = I_{det}/\eta$ where η is the detector sensitivity, which is at $\lambda = 13.55$ nm, $\eta = 0.25$ A/W.

Then the radiation power arriving at the detector is

$$P_{det} = I_{det}/\eta = 5.5 \cdot 10^{-5}/0.25 = 2.2 \cdot 10^{-4}\,\text{W}.$$

Taking into account the transmission coefficients of the pair of filters ($T_{13.55} = 0.47$), the power arriving at the exposed sample is

$$P_{sample} = P_{det}/(T_{13.55})^2 = 2.2 \cdot 10^{-4}/(0.47 \cdot 0.47) = 1.0 \cdot 10^{-3}\,\text{W}.$$

For patterning, a mesh with period 0.5 mm and bridge width 0.05 mm was used in the film sample as a mask for partial masking of the surface. Photographs of the sample holder with attached mesh and sample are shown in Figure 5.

2. Findings and discussion

TinS and TOC-21 oxo clusters contain 12 and 14 tin atoms in their molecules, respectively. Tin refers to a group of metals with high atomic numbers and has high absorption coefficient in interaction with EUV photons [18]. This makes the given compounds potentially promising for creating resistive materials both for electron-beam and EUV nanolithography. Due to introduction of metal atoms, etching resistance of a metal-containing resist increases compared with polymer resists, therefore it is preferable to produce thin films on the basis of obtained compounds (according to the literature — less than 40–50 nm), which is an advantage in the EBL and EUVL processes [3,33,34]. Therefore, the first investigation stage shall estimate the possibility and determine conditions of producing thin cluster films on single crystal silicon wafers.

60 nm films were deposited from TOC-21 solution in 2-butanone on a single crystal silicon wafer at a spin coater speed of 3000 rpm. The obtained films had uneven surface, which can be clearly seen on the AFM and SEM images (Figure 6). Agglomerates with sizes from 50 nm to 500 nm were observed on the sample surfaces. These agglomerates were probably caused by crystallization of TOC-21 on the wafer surface during film formation. Film surface roughness on the $2 \times 2\,\mu$m fragment was more than 3 nm. The data are shown in Table 1.

Replacement of 2-butanone with ethyl lactate in the TOC-21 case made it possible to avoid large crystalline agglomerates on the wafer surface and to obtain films with

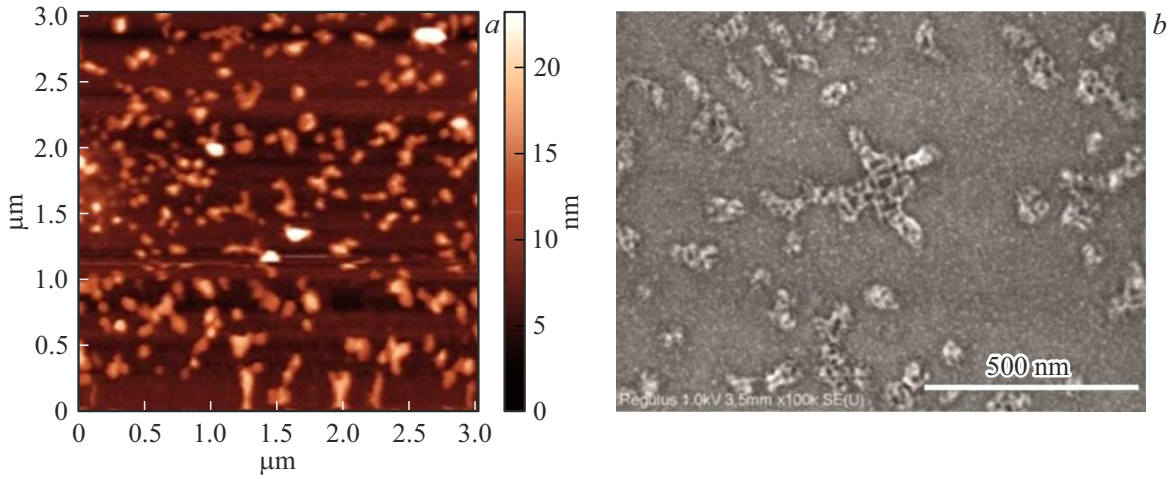

Figure 6. AFM (*a*) and SEM (*b*) images of film obtained from TOC-21 solution in 2-butanone ([TOC-21] = 13 g/l, 3000 rpm).

Table 1. Influence of the origin of solvent and spin coater speed on the thickness and surface roughness (R_q) of films obtained from TOC-21 and TinS

Compound	Concentration (solvent), g/l	Speed, rpm	d, nm	R_q, nm
TOC-21	13 (2-butanone)	3000	60	3.3
	7.75 (ethyl lactate)	300	40^1-30^2	0.6
		500	25	2.3
		1000	15	2.8
		2000	10	3.2
TinS	5.0 (2-butanone)	500	50	7.5
		1000	45	11.2
		2000	40^3	13

Note. [1] — film 1, [2] — film 2, [3] — film 3.

more uniform surface. Film thickness was set by the spin coater speed during coating deposition in the range from 300 rpm to 2000 rpm (Table 1). From the shown data it can be seen that an increase in speed from 300 rpm to 2000 rpm leads to a decrease in film thickness by 3–4 times from 40–30 nm to 10 nm. Whilst R_q of TOC-21 films increases from 0.6 nm to 3.2 nm.

Figures 7 and 8 show AFM and SEM images of surfaces of the obtained films.

Also, 40–50 nm films were formed from TinS solution in 2-butanone at various spin coater speeds (Table 1). Film surface uniformity degrades considerable as the film thickness decreases. TinS film roughnesses nearly double from 7.5 nm to 13 nm.

Thus, films formed from TinS solution in 2-butanone have much higher surface roughnesses compared with films obtained from TOC-21 solutions in ethyl lactate. Note that to determine R_q , a fragment without pronounced nonuniformities was deliberately chosen on the film surface. But analysis of the whole surface of samples obtained from TinS showed the following picture. Figure 9 shows microphotographs of TinS film surfaces (spin coater speeds are 500 rpm, 1000 rpm and 2000 rpm) made using an optical microscope. It can be seen that as the speed decreases from 2000 rpm to 1000 rpm, star-shaped nonuniformities with sizes of tens of microns occur on the film surface. Further decrease in speed to 500 rpm leads to an increase in the amount of nonuniformities and their considerable enlargement. It can be believed that they consist of TinS oxo cluster microcrystal agglomerates. The presence of nonuniformities on the surface of film deposited at 500 rpm is also recorded by the AFM technique (Figure 10). AFM image of the film surface also shows individual nonuniformities with sizes of the order of 10 μm.

Thus, TOC-21 films deposited on single crystal silicon wafers from oxo cluster solution in ethyl lactate show the best morphological characteristics in the given film

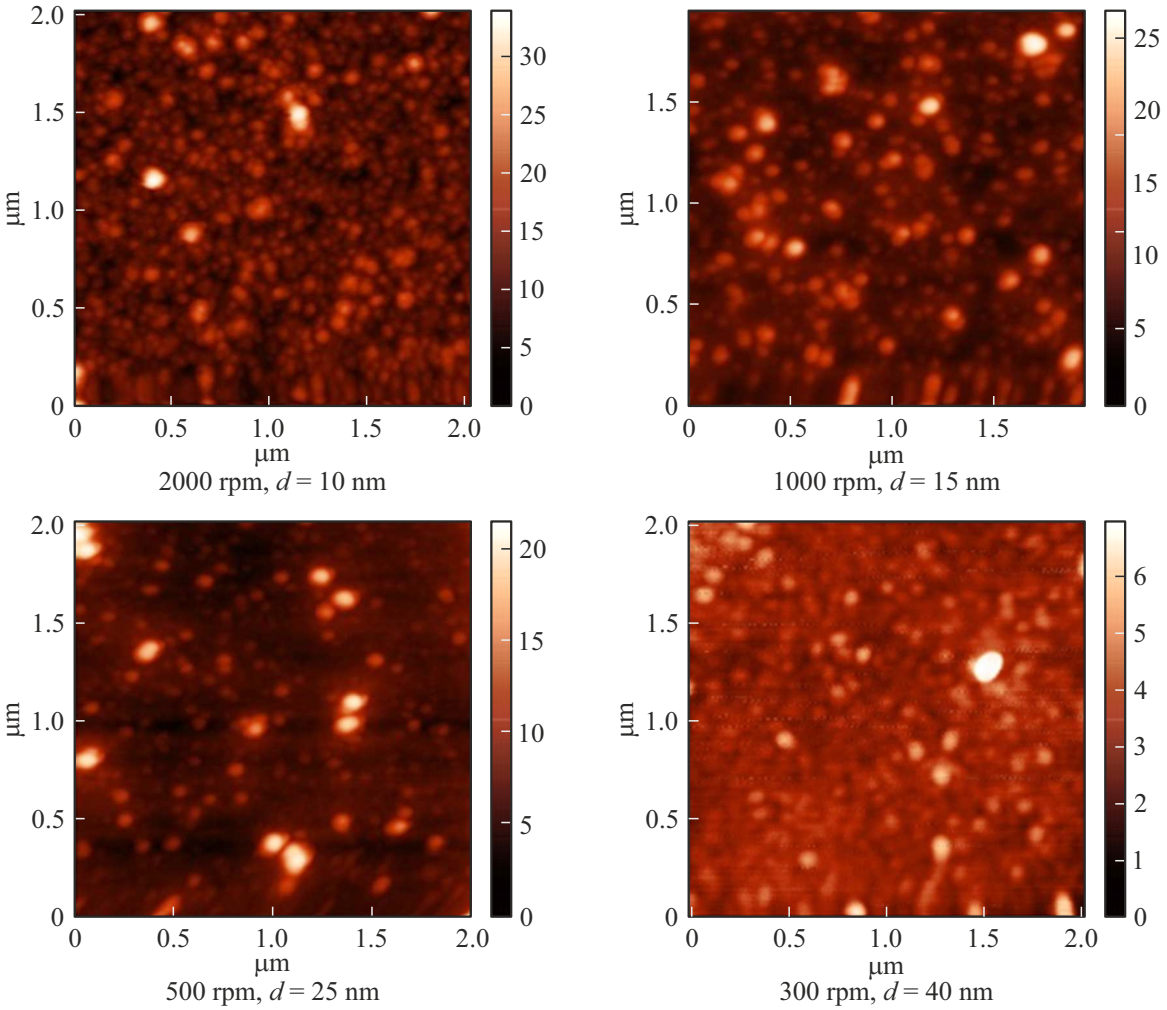

Figure 7. AFM surface images of TOC-21 films deposited on a wafer from ethyl lactate solution at different spin coater speeds. [TOC-21] = 7.75 g/l.

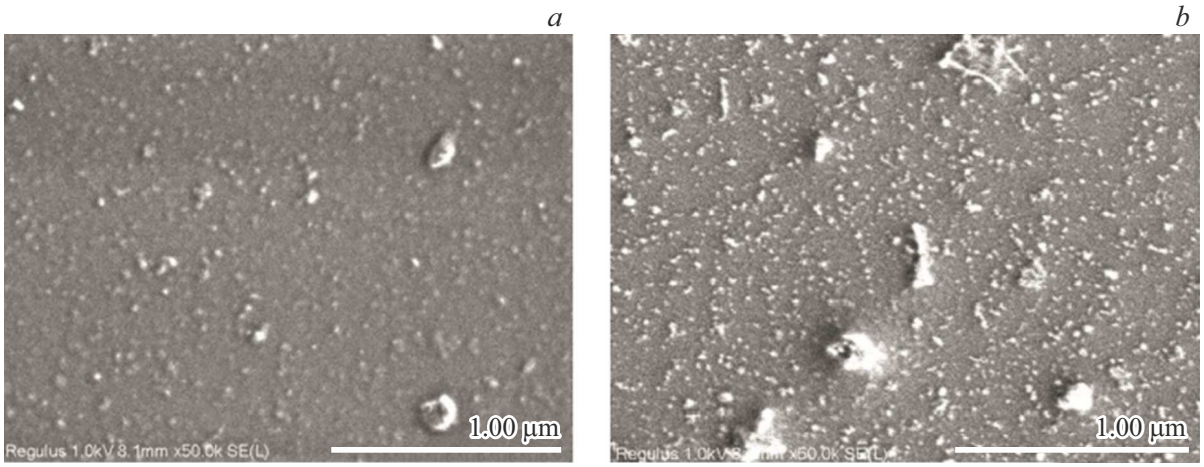

Figure 8. SEM surface images of TOC-21 films deposited on a wafer from ethyl lactate solution at different spin coater speeds: *a* — 300 rpm (40 nm) and *b* — 1000 rpm (16 nm); [TOC-21] = 7.75 g/l. Approximation 50 000 x

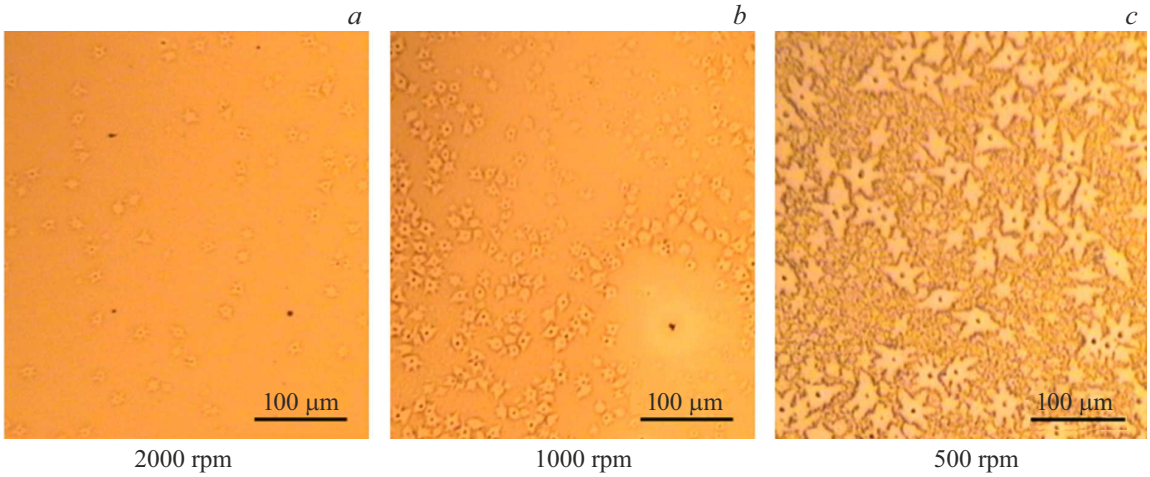

Figure 9. Microphotographs of TinS films on the wafer surface (2-butanone solvent) at various spin coater speeds. LOMO MSP-1 microscope.

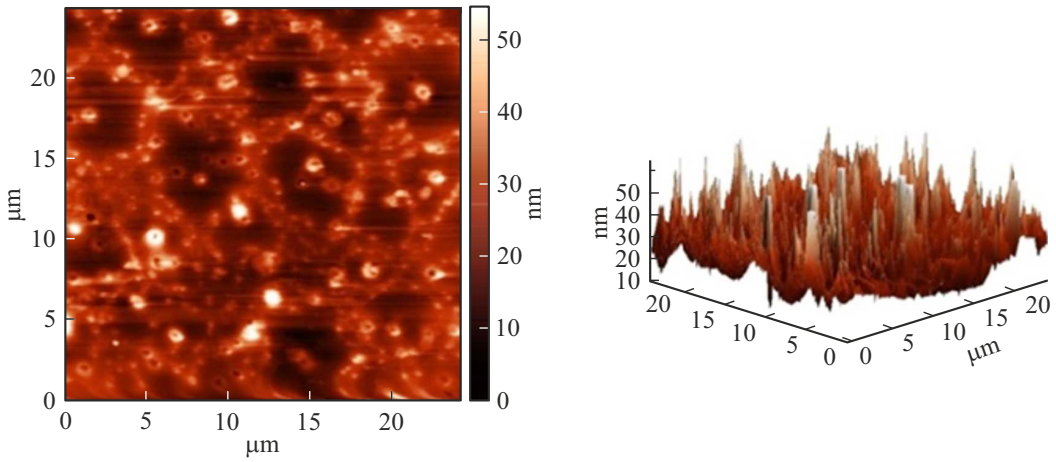

Figure 10. AFM surface images of TinS film (2-butanone solvent) deposited on a wafer at a speed of 500 rpm.

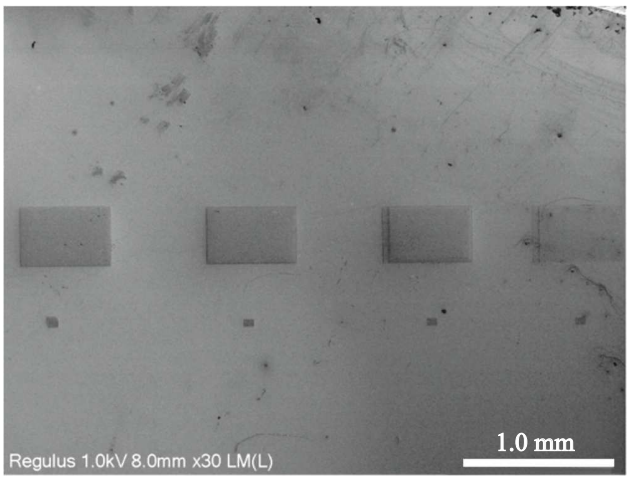

Figure 11. SEM surface image of wafer with film 1 after electron-beam exposure using SEM and subsequent development. Electron-beam exposure time and conditions: upper row (250 x magnification) and lower row (2500 x magnification) left to right — 60 min., 30 min., 15 min. and 7.5 min.

formation conditions compared with TinS films. Thickness-/roughness-optimal films are formed by deposition on wafer at a spin coater speed of 300–1000 rpm.

The second investigation stage included evaluation of sensitivity of obtained films to electron-beam and extreme ultraviolet radiation in order to test them for further investigations aimed at creating resistive materials.

Surface of wafer with film 1 was exposed to electron beam using the Regulus SU8100 (Hitachi, Japan) scanning electron microscope (experiment conditions are shown in the experimental part). Electron-beam exposure times (Figure 11 left to right) are 60 min, 30 min, 15 min and 7.5 min. As can be seen (Figure 11), electron-beam exposure of film 1 followed by development creates well-shaped structures in the exposed regions on the wafer surface. Energy-dispersive analysis of the obtained structures (Figure 12) detects signals typical of tin, oxygen and silicon. Table 2 gives atomic and mass concentrations corresponding to these elements depending on the exposure time.

Table 2 shows that there is no signal from tin in the unexposed area of film 1 after development. This

Table 2. Atomic and mass concentrations of elements on the surface of structures obtained on the single crystal silicon wafer with film 1 depending on the electron-beam exposure time

Exposure, min	Atomic concentration, %			Mass concentration, %		
	O	Si	Sn	O	Si	Sn
–	1.35	98.65	0.00	0.78	99.22	0.00
7.5	1.71	98.22	0.06	0.98	98.75	0.27
15	3.01	96.76	0.23	1.72	97.30	0.98
30	3.67	95.93	0.40	2.10	96.22	1.68
60	3.43	96.16	0.41	1.96	96.32	1.72

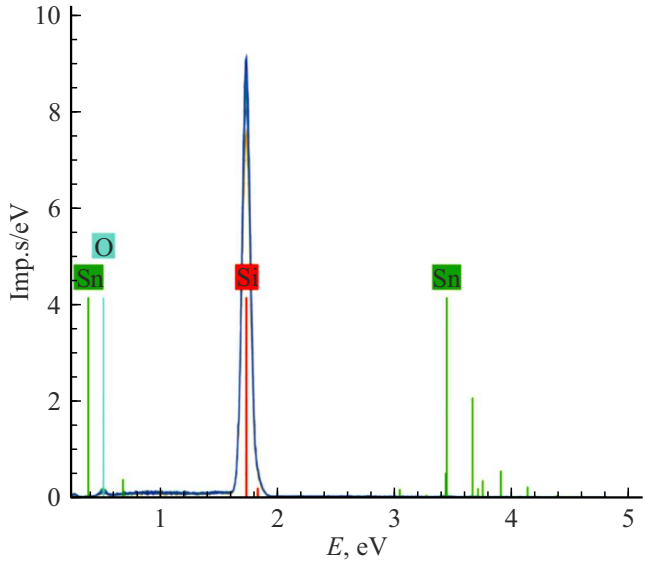

Figure 12. EDS spectrum of structures obtained on the wafer with film 1 after electron-beam exposure using SEM and subsequent development.

indicates that film 1 was completely removed from the unexposed wafer surface area during development. Tin signal, mass concentration 0.27 mass%, is observed in the area of film 1 irradiated during 7.5 min and developed. Increase in irradiation time of film 1 from 7.5 min to 30 min leads to gradual growth of tin atom concentration at the interfaces of exposed fragments from 0.27 mass% to 1.68 mass%. Oxygen concentration increases in the same way. This effect is probably related to formation of tin oxide under the action of electron beam. Increase in exposure time from 30 min to 60 min doesn't lead to significant formation of additional amounts of tin oxide.

To find structure formation conditions under the action of $\lambda = 13.55$ nm EUV radiation, films obtained from TOC-21 (film 2, $d = 30$ nm) and TinS (film 3, $d = 40$ nm) were tested. Exposure of film 2 to $\lambda = 13.55$ nm radiation during 10 min, 20 min, 40 min, 60 min, 90 min and 120 min has shown that the minimum exposure dose, at which changes in the surface morphology of the exposed film area are noticeable, is $D = 752$ mJ/cm^2 (60 min of exposure). Note that the recorded exposure region has no distinct boundaries and cannot be detected after development. Increase in the exposure time to 90 min and 120 min has shown that exposed areas had more distinct boundaries. When the irradiation dose is 1512 mJ/cm^2, the exposed film region edges are distinct and retain the boundaries after development. Before development, the film surface area with modified morphology was approximately $370 \times 560\,\mu$m in size. After development of the sample, the area size remained unchanged. Irradiation doses and SEM images of exposed film surface regions before and after development are shown in Figure 13.

TinS-based film 3 on wafer was exposed to $\lambda = 13.55$ nm EUV in the same conditions during 10 min, 20 min, 40 min and 60 min. Irradiation doses and SEM images of exposed surface regions of wafer with film 3 before and after development are shown in Figure 14. Formation of film 3 area with modified morphology is observed during 20 min exposure (irradiation dose 252 mJ/cm^2) (Figure 14, *a*), however, it (area) disappears during development. The same picture is observed for exposure during 40 min (irradiation dose 500 mJ/cm^2) (Figure 14, *b*). Retained film area with modified morphology after development is recorded for exposure during 60 min (irradiation dose 752 mJ/cm^2). The size of developed structure on the wafer surface retains the size of the film area with modified morphology before development (Figure 14, *c*, *d*).

Thus, TinS-based films appeared to be most sensitive to $\lambda = 13.55$ nm EUV, however, with the same thicknesses TinS-based films have worse morphological characteristics of surface and high roughnesses compared with TOC-21-based films.

Conclusion

The study has identified conditions for producing thin (10–60 nm) films of tin-oxo cluster compounds of alkyl (TinS) and non-alkyl (TOC-21) types on the single crystal silicon wafer surface. Film thickness is determined by

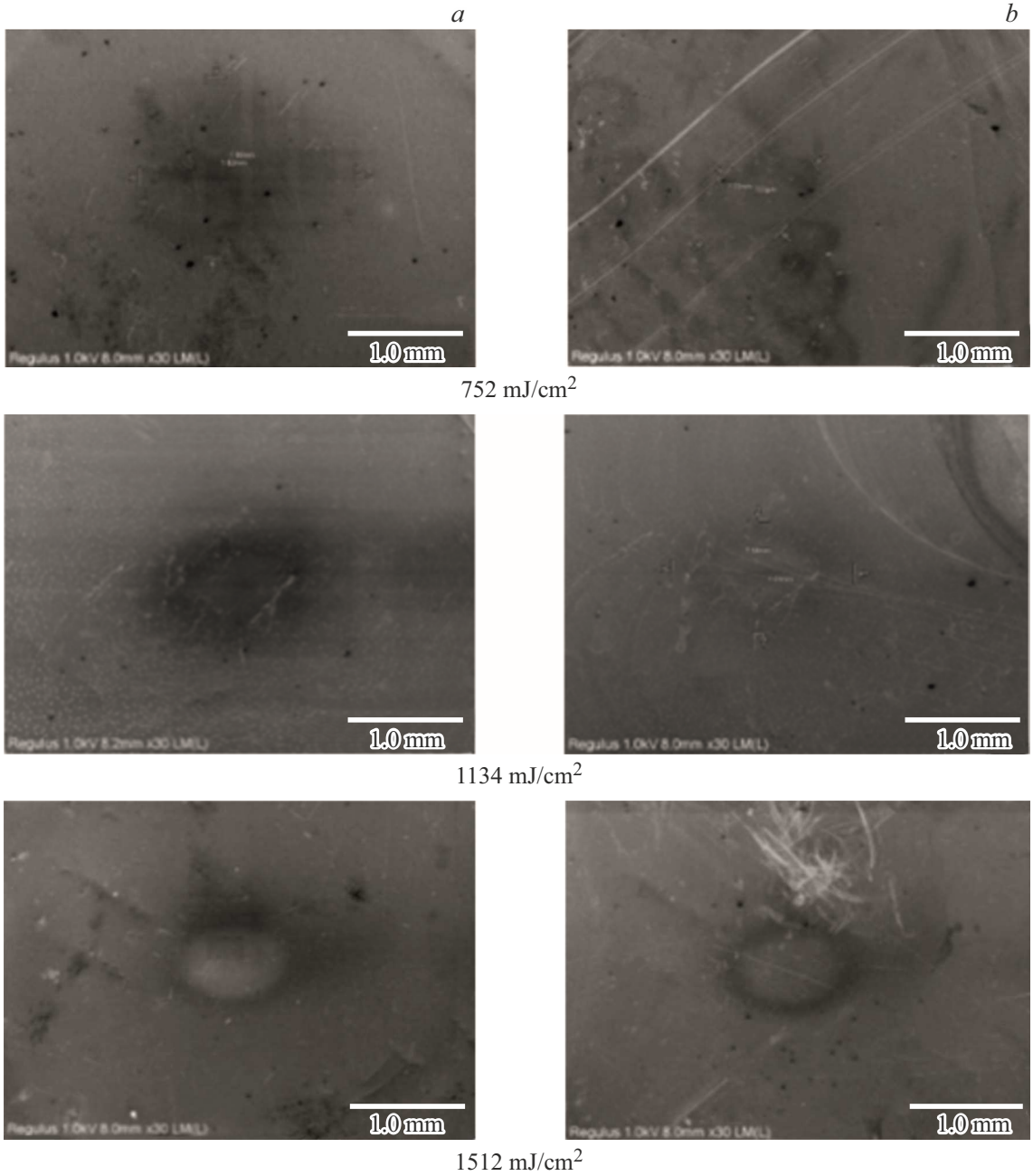

Figure 13. SEM surface images of the wafer with film 2 after $\lambda = 13.55$ nm EUV irradiation before (a) and after (b) development.

the origin of oxo cluster and solvent, and wafer speed. For TOC-21, 20−40 nm films with surface roughness less than 1 nm were obtained. For a wafer with TOC-21-based film, possibility of patterning from a tin-containing substance on the surface under electron-beam exposure is shown. Sensitivity of TinS and TOC-21 films to extreme ultraviolet radiation ($\lambda = 13.55$ nm) is also shown. Estimating comparison of EUV sensitivity of the tested samples and HSQ shows that sensitivity of TinS and TOC-21 oxo cluster films is much lower. At the same time, decrease in the Sn–C bond energy in an oxo cluster molecule due to a change in the origin of the oxo cluster shall increase the sensitivity to electron-beam and EUV radiation of a material based on such oxo cluster. Thus, the obtained data suggest that further studies of synthesis of new organotin-oxo clusters and creation of thin-film negative resists based on these clusters for EBL and EUVL have good prospects.

Funding

The study was carried out within the state assignment of the Institute of Organometallic Chemistry of RAS using the equipment provided by the Analytical Center of the Institute of Organometallic Chemistry named after G.A.Razuvaev and equipment provided by the Common Use Center of the

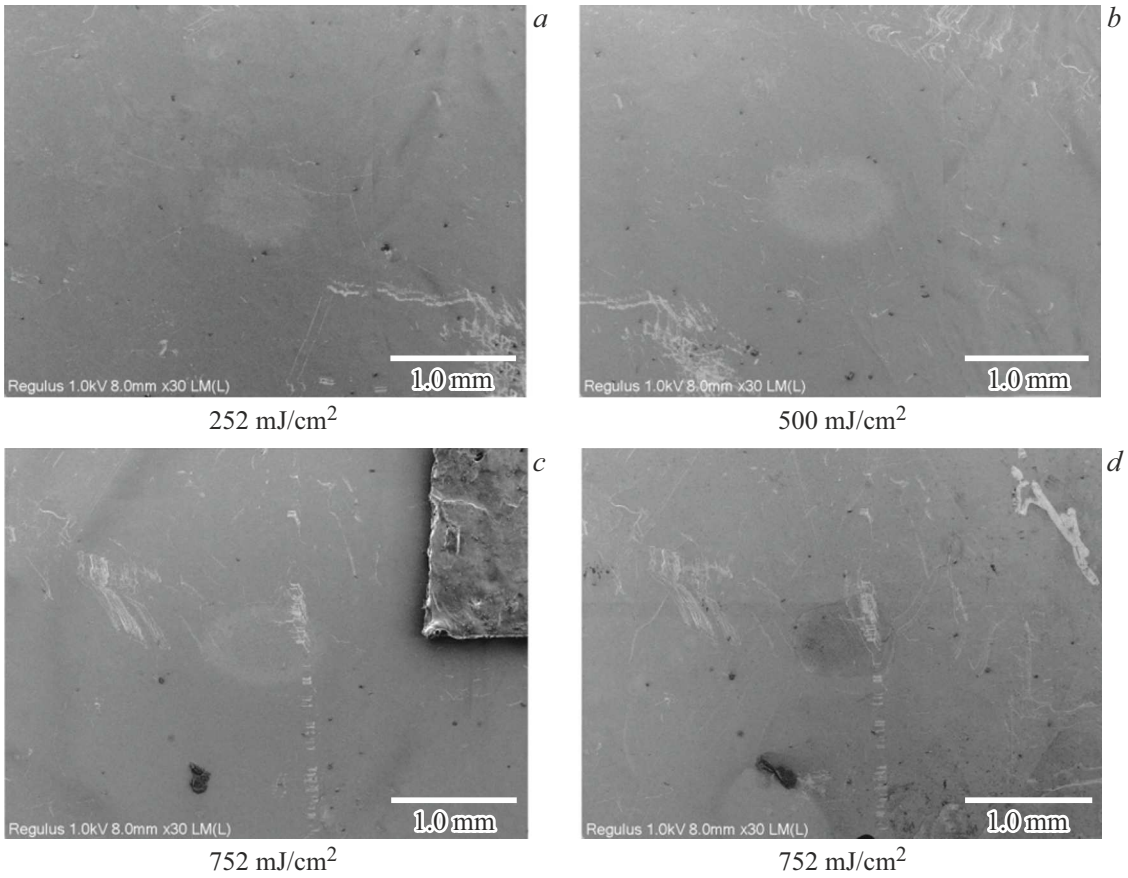

Figure 14. SEM surface images of the wafer with film 3 after $\lambda = 13.55$ nm EUV irradiation before $(a-c)$ and after (d) development.

Institute for Physics of Microstructures of RAS „Physics and Technology of Microstructures".

Conflict of interest

The authors declare no conflict of interest.

References

[1] N. Mojarad, J. Gobrecht, Y.Ekinci. Scientific Reports, **5**, 9235 (2015). DOI: 10.1038/srep09235
[2] R. Fallica, J.K. Stowers, A. Grenville, An. Frommhold, A.P.G. Robinson, Ya. Ekinci. J. Micro/Nanolith., MEMS MOEMS, **15** (3), 033506 (2016). DOI: 10.1117/1.JMM.15.3.033506
[3] T. Manouras, P. Argitis. Nanomaterials, **10**, 15932 (2020). DOI: 10.3390/nano10081593
[4] Dow Corning XR-1541 E-Beam Resist Product Information.
[5] H. Namatsu, T. Yamaguchi, M. Nagase, K. Yamazaki, K. Kurihara. Microelectron Eng., **41**–**42**, 331 (1998). DOI: 10.1016/S0167-9317(98)00076-8
[6] H. Namatsu, Y. Takahashi, K. Yamazaki, T. Yamaguchi, M. Nagase, K. Kurihara, J. Vac. Sci. Technol., **16** (B), 69 (1998). DOI: 10.1116/1.589837
[7] A.E. Grigorescu, M.C. van der Krogt, C.W. Hagen, P. Kruit. J. Vacuum Sci. Technol. B: Microelectronics and Nanometer Structures Processing, Measurement and Phenomena, **25** (6), 1998 (2007). DOI: 10.1116/1.2794316
[8] H. Duan, H. Hu, H.K. Hui, Z. Shen, J.K.W. Yang. Nanotechnology, **24** (18), 185301 (2013). DOI: 10.1088/0957-4484/24/18/185301
[9] A.E. Grigorescu, C.W. Hagen. Nanotechnology, **20**, 292001 (2009). DOI: 10.1088/0957-4484/20/29/292001
[10] V. Sidorkin, A. Grigorescu, H. Salemink, E. Drift. Microelectronic Engineering, **86**, 749 (2009). DOI: 10.1016/j.mee.2008.12.071
[11] A.A. Tatarintsev, A.V. Shishlyannikov, K.V. Rudenko, A.E. Rogozhin, A.E. Ieshkin. Mikroelektronika, **49** (3), 163 (2020) (in Russian). DOI: 10.31857/S0544126920030060
[12] G.M. Schmid, L.E. Carpenter, J.A. Liddle. J. Vac. Sci. Technol., **22** (6), 3497 (2004). DOI: 10.1116/1.1825014
[13] M. Haffner, A. Haug, A. Heeren, M. Fleischer, H. Peisert, T. Chaasse, D.P. Kern. J. Vac. Sci. Technol., **25** (6), 2045 (2007). DOI: 10.1116/1.2794324
[14] S. Choi, N. Jin, V. Kumar, M. Shannon, I. Adesida. J. Vac. Sci. Technol., **25** (6), 2085 (2007). DOI: 10.1116/1.2794315
[15] A.V. Myakonkikh, A.V. Shishlyannikov, A.A. Tatarintsev, V.O. Kuzmenko, K.V. Rudenko, E.S. Gornev. Mikroelektronika, **50** (5), 333 (2021) (in Russian). DOI: 10.31857/S0544126921050045

[16] A.V. Myakonkikh, N.A. Orlikovsky, A.E. Rogozhin, A.A. Tatarintsev, K.V. Rudenko. Mikroelektronika, **3** (179), (2018) (in Russian). DOI: 10.7868/S0544126918030018
[17] I. Junarsa, M.P. Stoykovich, P.F. Nealey, Y. Ma, F. Cerrina. J. Vac. Sci. Technol., **23** (1), 138 (2005). DOI: 10.1116/1.1849213
[18] Electronic source. Available at: http://www.cxro.lbl.gov
[19] B. Cardineau, R. Del Re, M. Marnell, H. Al-Mashat, M. Vockenhuber, Y. Ekinci, C. Sarma, D.A. Freedman, R.L. Brainard. Microelectronic Engineering, **127**, 44 (2014). DOI: 10.1016/j.mee.2014.04.024
[20] C. Eychenne-Baron, F. Ribot, C. Sanchez. J. Organometallic Chem., **567**, 137 (1998). DOI: 10.1016/S0022-328X(98)00676-7
[21] J. Haitjema, L. Wu, A. Giuliani, L. Nahon, S. Castellanos, A.M. Brouwer. Phys. Chem. Chem. Phys., **23**, 20909 (2021). DOI: 10.1039/d1cp03148a
[22] D. Wang, Zh.-N. Chen, Q.-R. Ding, Ch.-Ch. Feng, S.-T. Wang, W. Zhuang, L. Zhang. CCS Chem., **2**, 2607 (2020). DOI: 10.31635/ccschem.020.202000546
[23] G. Lim, K. Lee, S. Choi, H.J. Yoon. Coordination Chem. Rev., **493**, 215307 (2023). DOI: 10.1016/j.ccr.2023.215307
[24] I. Bespalov, Y. Zhang, J. Haitjema, R.M. Tromp, S. Jan van der Molen, A.M. Brouwer, J. Jobst, S. Castellanos. ACS Appl. Mater. Interfaces, **12**, 9881 (2020). DOI: 10.1021/acsami.9b19004
[25] N. Thakur, L.-T. Tseng, M. Vockenhuber, Ya. Ekinci, S. Castellanos. J. Article Open Access Open Access J. of Micro/Nanolithography, MEMS, and MOEMS, 18 (4), 43504 (2019). DOI: 10.1117/1.JMM.18.4.043504
[26] L. Wu, J. Liu, M. Vockenhuber, Y. Ekinci, S. Castellanos. Eur. J. Inorg. Chem., **2019** (38), 4136 (2019). DOI: 10.1002/ejic.201900745
[27] J. Haitjema, Y. Zhang, M. Vockenhuber, D. Kazazis, Y. Ekinci, A.M. Brouwer. J. Micro/Nanolith. MEMS MOEMS, **16**, 1 (2017). DOI: 10.1117/1.JMM.16.3.033510
[28] D. Wang, X. Yi, L. Zhang. Sci. China Chem., **65**, 114 (2022). DOI: 0.1007/s11426-021-1092-2
[29] F. Wu, B.J. Harper, D.A. Marsh, S. Saha, T. Diulus, J.M. Amador, D.A. Keszler, G.S. Herman, B.L.S. Maddux, S.L. Harper. Environ Toxicol Chem., **38**, 2651 (2019). DOI: 10.1002/etc.4580
[30] Electronic source. Available at: https://henke.lbl.gov/optical_constants/filter2.html
[31] A.Ya. Lopatin, V.I. Luchin, A.N. Nechai, A.A. perekalov, A.E. Pestov, D.G. Reunov, N.I. Chkhalo. ZhTF, **94** (8), 1323 (2024) (in Russian). DOI: 10.61011/JTF.2024.08.58560.142-24
[32] P.N. Aruev, M.M. Barysheva, B.Ya. Ber, N.V. Zabrodskaya, V.V. Zabrodskii, A.Ya. Lopatin, A.E. Pestov, M.V. Petrenko, V.N. Polkovnikov, N.N. Salashchenko, V.L. Sukhanov, N.I. Chkhalo. Quant. Electron, **42**, 943 (2012). DOI: 10.1070/QE2012v042n10ABEH014901
[33] A. Grenville, J. Anderson, B. Clark, P. De Schepper, J. Edson, M. Greer, K. Jiang, M. Kocsis, S. Meyers, J. Stowers, A. Telecky, D. De Simone, G. Vandenberghe. In: Proceedings of SPIE — The International Society for Optical Engineering, **9425**, 94250S (2015). DOI: 10.1117/12.2086006
[34] D.De Simone, Y. Vesters, G. Vandenberghe. Advanced Opt. Technol., **6** (3–4), 163 (2017). DOI: 10.1515/aot-2017-0021

Translated by E.Ilyinskaya